Journal of Physics: Conference Series **2191** (2022) 012014 doi:10.1088/1742-6596/2191/1/012014

Echoes from the event horizon of a superfluid vortex

K Güven[1] **and B Demirkaya**[2]

[1]Department of Physics, Koç University, Istanbul, Turkey
[2]Department of Physics, Izmir Institute of Technology, Izmir, Turkey

E-mail: kguven@ku.edu.tr

Abstract. A vortex formed in the superfluid state of a Bose-Einstein condensate may exhibit superradiance à la blackhole for radially propagating acoustic fluctuations. The analogy is usually based on the so-called draining bathtub model of the vortex, in which an event horizon and ergosphere emerges when the radial velocity of the superfluid exceeds the propagation speed of sound in the condensate. The acoustic fluctuations mimic a massless scalar field in the curved Lorentzian space-time of the vortex and are governed by the Klein-Gordon wave equation. One common main approximation is the constant background density of the superfluid even in the presence of the vortex. This sets a constant relativistic sound speed. However, the vortex state solution of the Gross-Pitaevskii equation clearly shows that both the density and the speed of sound vary radially near the vortex core, where the event horizon and thus the superradiance will take place. What changes would this complex interdependence bring to the formulation and to the outcomes of the superradiance based on constant density approximation? Here, we recount this question posed under the guidance of Prof. Tekin Dereli and present recent results. We show that the self-consistent density modifies the amplification dynamics near the event horizon significantly, thereby altering the temporal and spectral fingerprint of the superradiance of the vortex.

1. Introduction

The superfluid Bose-Einstein condensates demonstrated great potential to investigate physical phenomena arising from black-holes analogously in the laboratory environment [1, 2, 3, 4]. The similarity of the formulation for the propagation of electromagnetic waves in gravitational fields and for the acoustic waves in moving fluids provides a mapping of the dynamics [5]. The experimental realization of vortex states in rotating trapped atomic BECs [6, 7], brought the acoustic black-hole analogy into the BEC superfluid [8, 2]. The acoustic superradiance and even the Penrose process in both BEC superfluids and classical fluids have been suggested in the literature [9, 10, 11], and quickly gained momentum as an active research subject. Eventually, an acoustic black hole in a needle-shaped BEC of 87Rb is experimentally demonstrated and recently spontaneous Hawking radiation, stimulated by quantum vacuum fluctuations, emanating from an analogue black hole in an atomic BEC is reported [12, 13, 14].

Theoretical/numerical studies concerning acoustic superradiance mostly investigated linear acoustic perturbations superimposed on a *constant* background density of the superfluid [9, 11, 15, 16, 17]. On one hand, the constant background density approximation (const-bg-dens) combined with the draining bathtub model (DBT) [18], elegantly demonstrates the acoustic superradiance. On the other hand, the BEC theory indicates that the self-consistent background density profile of the superfluid (self-bg-dens) in the vicinity of the vortex is not constant [19].

This begs the question how good the const-bg-dens approximation captures the superradiance dynamics. Here, we present a comparative numerical study of the acoustic superradiance in the const-bg-dens and in the self-bg-dens models to address this question. First and foremost, the self-bg-dens formulation introduces a *radially varying relativistic speed* near the vortex, as opposed to it being a *constant*. This fact changes the acoustic black-hole portrait entirely. In the absence of a constant relativistic speed, scale-independence is lost. Indeed, the formulation reveals interdependencies among the rotating vortex parameters and the black-hole parameters, that do not appear under the const-bg-dens approximation. For multi-quantized vortex states, this would imply further complications as the self-bg-dens changes with the vortex quantization number. We should however note that, at present, the stability and experimental realization of multiquantized vortices is challenging and still under progress.

There are two shortcomings of the present work we should mention at the onset, and point the reader to the backing literature where available: (1) The dispersion of acoustic perturbations is not included, although they are inherent. We can probably get away (but not too far!) by arguing that it restricts the applicability of the model to weak-dispersive systems. A recent study [20] investigated acoustic superradiance with Bogoliubov dispersion and with the const-bg-dens approximation and concluded the following: (i) For weak dissipations the superradiance occurs at all frequencies of the acoustic fluctuations below the angular frequency of the vortex. This condition is the same as in the const-bg-dens and self-bg-dens cases. (ii) For strong dispersion, the superradiance may cease to exist below a critical rotation frequency of the vortex. We can speculate that this condition would emerge similarly in the present work when dispersion is included. (2) The BEC superfluid is assumed to be unconfined, which is not the case under experimental conditions. Again, one may assume that the variation of the confinement potential within the characteristic length scales of the acoustic scaterring from the vortex is negligible, and that the boundaries of the confinement are sufficiently far away from the vortex to interfere.

With this setting, the rest of the paper is organized as follows: In section 2 we recapitulate the vortex state formulation of the BEC superfluid. This is followed by the Klein-Gordon equation for the propagation of acoustic linear perturbations as section 3. The numerical implementation is described in section 4 and the results are given in section 5. Last section concludes the study.

2. The vortex state of an unconfined BEC

The evolution of the wavefunction of the bosons is governed by the Gross-Pitaevskii equation

$$i\hbar\frac{\partial\Psi(\mathbf{x},t)}{\partial t}=\left(-\frac{\hbar^2}{2m}\nabla^2+V_{ext}+U_0\left|\Psi\right|^2\right)\Psi(\mathbf{x},t) \tag{1}$$

where V_{ext} is the external confining potential (set to zero in this study) and $V_H=\frac{4a\pi\hbar^2}{m}\left|\Psi\right|^2\equiv U_0\left|\Psi\right|^2$ is the repulsive Hartree potential, with a scattering length, a. Steady state solutions can be expressed as $\Psi(\mathbf{x},t)=\psi(\mathbf{x})e^{-i\mu t/\hbar}$, where $\mu=\frac{\hbar^2}{2m\xi^2}$ is the chemical potential expressed in terms of the healing length $\xi=\sqrt{\frac{\hbar^2}{2\rho_\infty mU_0}}$. This is a characteristic length scale in which the condensate density tends to its bulk value $\rho_\infty=\left|\psi(r\to\infty)\right|^2$.

2.1. Density profile of the vortex

For the vortex state, we seek a steady state axisymmetric solution of Eq.1 with the spatial part expressed in polar coordinates in the form

$$\psi(\mathbf{x})=f_q(r)e^{iq\theta}, \tag{2}$$

Here, $f_q(r)$ is the radial profile and the integer q denotes the winding (quantization) number of the vortex. Introducing dimensionless radial coordinate $\tilde{r}=r/\xi$ and the scaled function

$\chi_q = f_q/\sqrt{\rho_\infty}$ Eq.1 yields

$$-\frac{1}{\tilde{r}}\frac{d}{d\tilde{r}}\left(\tilde{r}\frac{d\chi_q}{d\tilde{r}}\right) + \frac{q^2\chi_q}{\tilde{r}^2} + \chi_q^3 - \chi_q = 0. \tag{3}$$

Equation 3 is subject to the boundary conditions $\chi_q(0) = 0, \chi_q(\infty) = 1$.

In the absence of the confinement of the condensate, multiquantized ($q > 1$) vortex states are unstable and decay into single quantized vortices[21, 22]. Experimentally obtained cigar-shaped condensates did not exhibit multiquantized vortices, either[23, 24]. Thus, while there has been theoretical[25] and experimental[26] effort to realize multiquantized vortices in different confinement potentials, the dynamical stability is an issue. The present work will consider the single-quantized ($q = 1$) case only.

The density profile dictated by Eq.3 has no closed form solution. In order to proceed with the analytical formulation of the metric and the solution of the Klein-Gordon equation, one has to resort to an approximate functional form. These were reported in the literature [27, 28, 29, 30], from which we pick the following functional form[29].

$$\chi_1 = \sqrt{\frac{\tilde{r}^2}{2+\tilde{r}^2}}, \tag{4}$$

It should be stressed that this approximation underlies the entire subsequent formulation and its results. Figure1 compares the numerical solution of Eq.3 with the function4. The background

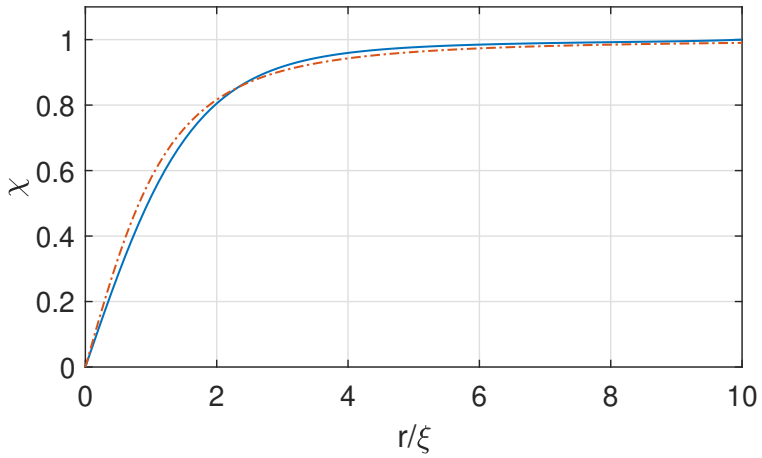

Figure 1: The numerical (solid) and approximate functional form (dash-dotted) of the radial wave function $\chi(r/\xi)$.

density profile of the vortex is then found from $\rho(r) = |\psi(r,\theta)|^2$

$$\rho_0(r) = \rho_\infty \frac{(r-r_0)^2}{(r-r_0)^2 + 2\xi^2} \tag{5}$$

where r_0 is the vortex center. The propagation speed of sound in the BEC is defined by the density $c = \sqrt{U_0\rho/m}$ and becomes

$$c(r) = c_\infty \sqrt{\frac{(r-r_0)^2}{(r-r_0)^2 + 2\xi^2}}, \tag{6}$$

where $c_\infty = \frac{\hbar}{m}\sqrt{4\pi a\rho_\infty}$ denotes the bulk value for the speed of sound.

Equations 5 and 6 comprise the key elements in the formulation of the vortex as an acoustic black hole. Their radial dependence becomes inherent in the superradiance dynamics.

2.2. Velocity profile of the vortex

At the vortex axis, the velocity of the condensate becomes singular. The consequence is that the circulation around a contour enclosing the vortex becomes nonzero and the velocity acquires a tangential component, described by a winding number.

$$\Theta = \oint \vec{v} \cdot \vec{dl} = 2\pi q \frac{\hbar}{m}, \qquad q = \pm 1, \pm 2... \tag{7}$$

$$v_{\hat{\phi}} = \frac{\Theta}{2\pi r}\hat{\theta} \equiv \frac{B}{r}\hat{\theta}. \tag{8}$$

Since the continuity equation $\frac{\partial \rho}{\partial t} + \nabla \cdot (\rho \vec{v}) = 0$, must be satisfied, the radial component of the velocity becomes

$$\nabla \cdot (\rho_0 \vec{v}) = 0 \Rightarrow v_{\hat{r}} = -\frac{A}{\rho(r) r} \tag{9}$$

where A is an empirical parameter to be set from experimental data (see section3.1). When contrasted with the velocity components of the draining bathtub model with a constant background density[31, 18], $\vec{v} = \frac{-A}{r}\hat{r} + \frac{B}{r}\hat{\theta}$ it is evident that the density modifies the radial velocity rather than being a mere scaling factor.

3. Acoustic Perturbations and the Klein-Gordon equation

For the superradiance, we consider small fluctuations superimposed on the background wavefunction $\psi = \psi_0 + \psi_1 = \sqrt{\rho} e^{i\Phi}$. With the linearized fluctuations in the density $\rho = \rho_0 + \rho_1$, and the phase $\Phi = \Phi_0 + \Phi_1$, substituting into Eq.1 yields the following set of equations

$$\frac{\partial \rho_1}{\partial t} + \frac{\hbar}{m} \nabla \cdot (\rho_0 \nabla \Phi_1) + \nabla \cdot (\rho_1 \vec{v}) = 0, \tag{10}$$

$$\partial_t \Phi_1 = -v \cdot \nabla \Phi_1 - U_0 \rho_1 + \frac{\hbar^2}{2m} D_2 \rho_1, \tag{11}$$

The velocity is expressed in terms of a "velocity potential" $\vec{v} = (\hbar/m)\nabla\Phi$. The last term in Eq.11 is known as the quantum pressure term[27] given explicitly below

$$D_2 \rho_1 = \frac{1}{2\sqrt{\rho_0}} \nabla^2 \frac{\rho_1}{\sqrt{\rho_0}} - \frac{\rho_1}{2\rho_0^{3/2}} \nabla^2 \sqrt{\rho_0}. \tag{12}$$

In the case of constant background density, this term can be neglected at all spatial ranges in comparison to other terms in Eq. 11, leading to the so-called hydrodynamic approximation. However, as the self-consistent density profile decays to zero at the vortex core, this simplification has to be justified in the vicinity of the event horizon. In the present study, we calculated and compared the respective magnitudes of the leading term in the quantum pressure and the Hartree potential $U_0\rho_1$ near the event horizon and verified its validity.

Equations 10 and 11 yield the Klein-Gordon equation for the propagation of phase perturbations:

$$\frac{\partial}{\partial t}\left[\frac{\rho_0}{c^2}\left(\frac{\partial \Phi_1}{\partial t} + \vec{v} \cdot \nabla \Phi_1\right]\right) - \nabla \cdot (\rho_0 \nabla \Phi_1) + \nabla \cdot \left[\frac{\rho_0}{c^2}\left(\frac{\partial \Phi_1}{\partial t} + \vec{v} \cdot \nabla \Phi_1\right)\right] = 0. \tag{13}$$

By employing the techniques discussed in Ref.s [15], [32], one can reduce the Klein-Gordon equation into a set of coupled first-order partial differential equations. First, the following functions are defined

$$\Phi_1 = \phi_1(t,r) e^{im\phi} e^{ikz} \qquad \Pi = \pi_1(t,r) e^{im\phi} e^{ikz} \qquad \Gamma = \gamma_1(t,r) e^{im\phi} e^{ikz} \tag{14}$$

where(k, m) denote the axial and azimuthal wave numbers. We take translational symmetry along vortex axis (i.e $k = 0$) and single quantized vortex ($m = 1$). These functions are then used to define the conjugate fields

$$\Gamma = \frac{\partial \Phi_1}{\partial x^i} \qquad\qquad \Pi = -\frac{1}{c}\left(\frac{\partial \Phi_1}{\partial t} - \beta^i \Gamma_i\right), \tag{15}$$

where $x_i = (r, \theta, z)$ denote the cylindrical coordinates and $\beta^i = (-\upsilon_r, -\upsilon_\theta/r, 0)$ are the velocity components. Finally, the radial parts of these functions satisfy the following set of coupled first-order partial differential equations

$$\frac{\partial \phi_1}{\partial t} = -c\pi_1 - \upsilon_r \gamma_1 - \frac{im\upsilon_\theta}{r}\phi_1 \tag{16}$$

$$\begin{aligned}\frac{\partial \gamma_1}{\partial t} =& -\frac{\partial c}{\partial r}\pi_1 - c\frac{\partial \pi_1}{\partial r} - \frac{\partial \upsilon_r}{\partial r}\gamma_1 - \upsilon_r \frac{\partial \gamma_1}{\partial r} \\ & - \frac{\partial \upsilon_\theta}{\partial r}\frac{im}{r}\phi_1 + \frac{im\upsilon_\theta}{r^2}\phi_1 - \frac{im\upsilon_\theta}{r}\frac{\partial \phi_1}{\partial r}\end{aligned} \tag{17}$$

$$\begin{aligned}\frac{\partial \pi_1}{\partial t} =& \pi_1\left(-\frac{\partial c}{\partial r}\frac{\upsilon_r}{c} - \frac{im\upsilon_\theta}{r} - \frac{1}{r}\frac{\partial (r\upsilon_r)}{\partial r}\right) - \upsilon_r \frac{\partial \pi_1}{\partial r} \\ & + \frac{\gamma_1}{c}\left(-\frac{c^2}{r} - \frac{c^2}{\rho}\frac{\partial \rho}{\partial r} + \frac{\upsilon_\theta^2}{r} + \upsilon_\theta \frac{\partial \upsilon_\theta}{\partial r}\right) - c\frac{\partial \gamma_1}{\partial r} \\ & + \frac{\phi_1}{c}\left(\frac{m^2c^2}{r^2} + c^2k^2 - \frac{im\upsilon_r}{r}\frac{\partial \upsilon_\theta}{\partial r} - \frac{im\upsilon_r\upsilon_\theta}{r^2}\right)\end{aligned} \tag{18}$$

The numerical part of the study given in Sec.4 involves solving this set of equations.

3.1. The Black Hole profile of the vortex

The Klein-Gordon equation given in Eq. 13 renders an axisymmetric space-time with the metric

$$ds^2 = \frac{\rho}{c}\left[-cdt^2 + (dr - \upsilon_r dt)^2 + (rd\theta - \upsilon_\theta dt)^2\right]. \tag{19}$$

The off-diagonal elements in Eq. 19 can be reduced by the following coordinate transformation

$$dt = dt^* - \upsilon_r / \left(c^2 - \upsilon_r^2\right) dr, \tag{20}$$

$$d\theta = d\theta^* - \upsilon_r\upsilon_\theta / \left(r\left(c^2 - \upsilon_r^2\right)\right) dr, \tag{21}$$

$$dr = dr^*, \tag{22}$$

which yields,

$$ds^2 = \left[\left(\upsilon^2 - c^2\right)dt^2 + \frac{c^2}{c^2 - \upsilon_r^2}dr^2 + r^2 d\theta^2 + 2\upsilon_\theta r dt d\theta\right]. \tag{23}$$

In the form above, the vanishing of the coefficient of dt^2 defines the ergosphere radius, r_e whereas the singularity of the metric determines the event horizon, r_h, in accordance with the Kerr black hole formulation in general relativity. In terms of the components of v given in Eq.s8, 9

$$\upsilon^2 - c^2 = 0 \Rightarrow \frac{A}{\rho_\infty c_\infty} - \frac{r_h^4}{\left(r_h^2 + 2\xi^2\right)^{3/2}} = 0 \tag{24}$$

$$v_r^2 - c^2 = 0 \Rightarrow \frac{A^2\left(r_e^2+2\xi^2\right)^2}{\rho_\infty^2 r_e^6} + \frac{B^2}{r_e^2} - \frac{c_\infty^2 r_e^2}{r_e^2+2\xi^2} = 0 \tag{25}$$

The coefficient A may be determined by setting the event horizon at unit healing length $r_h = \xi$:

$$A = \frac{\xi\rho_\infty c_\infty}{3^{3/2}} \qquad\qquad B = \frac{\hbar}{m}. \tag{26}$$

This is because the vortex core size of cold-atom gases in experimental studies is estimated to be of the order of healing length [33] (i.e. $\sim$ 100nm). Note that B follows from Eq.8. For an experimental correspondence, Table 1 lists the parameters of a BEC of Rb-87 atoms taken from Ref.s[19, 34] and the resulting black hole parameters for a vortex state. We note that r_e is calculated as the only positive real root of Eq.25. Figure 2, shows the speed of sound and the

Table 1: The experimental (Ref.s [19, 34]) parameters of a BEC of Rb-87 atoms and the calculated parameters of the black-hole vortex.

a	m	ρ_∞	c_∞	ξ	r_h	r_e
5.77nm	$1.44\times10-25$kg	$10^{21}\mathrm{m}^{-3}$	6.2×10^{-3}m/s	83nm	ξ	1.84ξ

radial velocity of the condensate fluid near the vortex. Vertical dashed lines indicate the event horizon and the ergosphere radii, respectively. Noteworthy is the decrease of the speed of sound from the ergosphere boundary to the event horizon (roughly within one healing length range) by more than 25%. This significant variation is expected to have an observable effect on the superradiance dynamics.

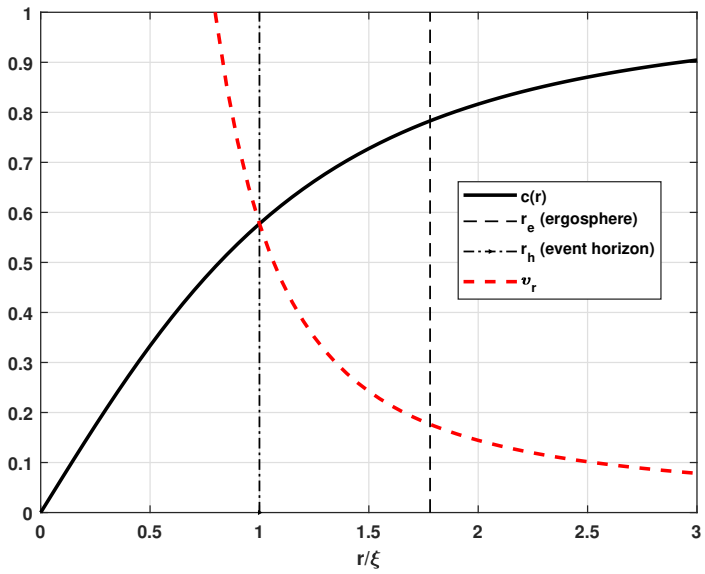

Figure 2: The speed of sound (Eq. 6), the radial velocity of the fluid (Eq. 9) along with the event horizon (r_h) and the ergoregion radius (r_e) calculated using the parameters given in Table 1.

4. Numerical Method

The propagation of the acoustic perturbations can be obtained by integrating the Eq.s 16, 17, 18. We employ Matlab's Partial Differential Equation Toolbox. The numerical calculations further implement the so-called "excision technique"[15, 35] to deal with the propagation through the event horizon and beyond numerically. From the calculated functions Π, Φ and Γ, we construct outgoing $(\Pi + \Phi)$ and incoming $(\Pi - \Phi)$ fields along the null ray. At large distances purely outgoing wave is implemented such that $\Gamma = \phi$. The spatiotemporal computational domain is defined as $0.5 < \tilde{r} < 110$, $0 < \tilde{t} < 110$, where $\tilde{r} = r/\xi$, $\tilde{t} = tc_\infty/\xi$ are dimensionless coordinates. The initial acoustic perturbation is defined in Eq. 14 as an axisymmetric, radially incoming Gaussian wave centered at r_0, with a width b as follows

$$\phi_1(0, r) = Nexp\left[-(r - r_0 + c(r)t)^2/b^2 - i\omega(r - r_0 + c(r)t)/c(r)\right]. \tag{27}$$

We set $r_0 = 50\xi$ and $b = 10\xi$. The initial π_1 and γ_1 are calculated by Eq.15. The main quantity we are interested in is the temporal variation of the energy of propagating acoustic perturbations,

$$E(t) = \int d^2r \frac{1}{2} M\rho \left|\vec{v}\right|^2 = (\hbar^2/2M) \int_0^{2\pi} d\theta \int_\xi^{r_{max}} \rho(r)(\nabla\Phi)^2 r dr, \tag{28}$$

with the scaled velocity

$$\vec{\tilde{v}} = -\frac{1}{3\sqrt{3}} \left(\frac{1}{\tilde{r}} + \frac{2}{\tilde{r}^3}\right) \hat{r} + \frac{\sqrt{2}}{\tilde{r}} \hat{\theta}. \tag{29}$$

5. Results: Temporal and spectral features of superradiance

We begin with the demonstration of the superradiance by contrasting the scattering of acoustic perturbations (density fluctuations ρ_1) from the event horizon of a vortex with (a) $m = 1$ and (b) $m = 0$ v(right panel) in Fig. 3 under const-bg-dens approximation. The self-bg-dens case is not shown as it is very similar to the const-bg-dens case in this plot type. At $t = 100 * c/a$ (the

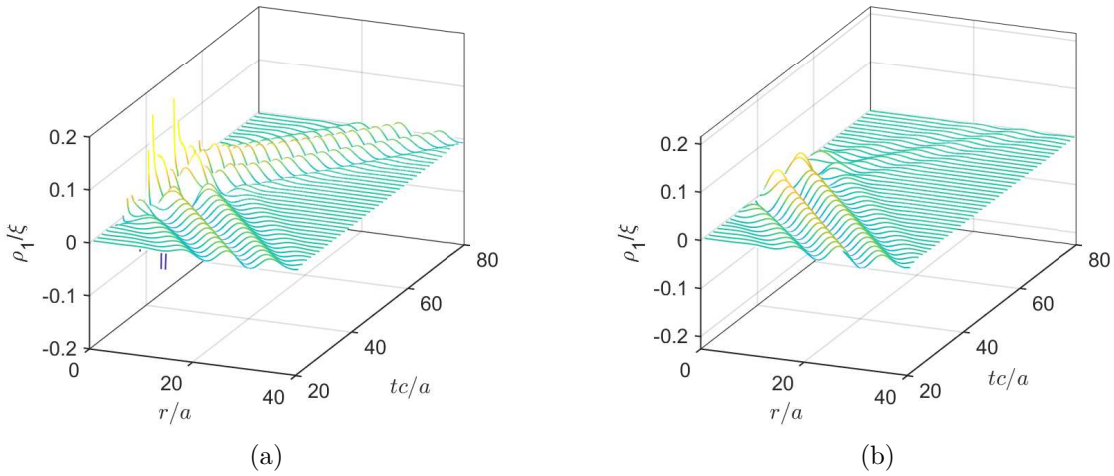

Figure 3: Propagation of the density fluctuations (ρ_1) in the scaled $r - t$ plane for (a) the superradiant ($m = 1$) and (b) the subradiant [$m = 0$)) settings of the vortex. The perturbation interacts with the event horizon between $t * c/a = 40$ and 60.

upper edge of the figures) the reflected wave returns to the launch point at $r_0 = 50\xi$. There is a clear difference between the superradiant and subradiant reflected profiles.

For a better representation in the self-bg-dens case, the bulk-normalized background density profile (Eq. 5) without and with the acoustic fluctuations at $t * c/a = 50$ superimposed are plotted in Fig. 4. For visibility, the profiles are cut out in an angular range and the profile with fluctuations is shifted vertically. The event horizon located at $\rho_0 = 0.5$ (see Fig. 3) remains just below the plotted range. The fluctuations against the rapidly decaying background density near the event horizon are hardly noticeable, but they are prominent near the ergosphere $r/a \sim 2$.

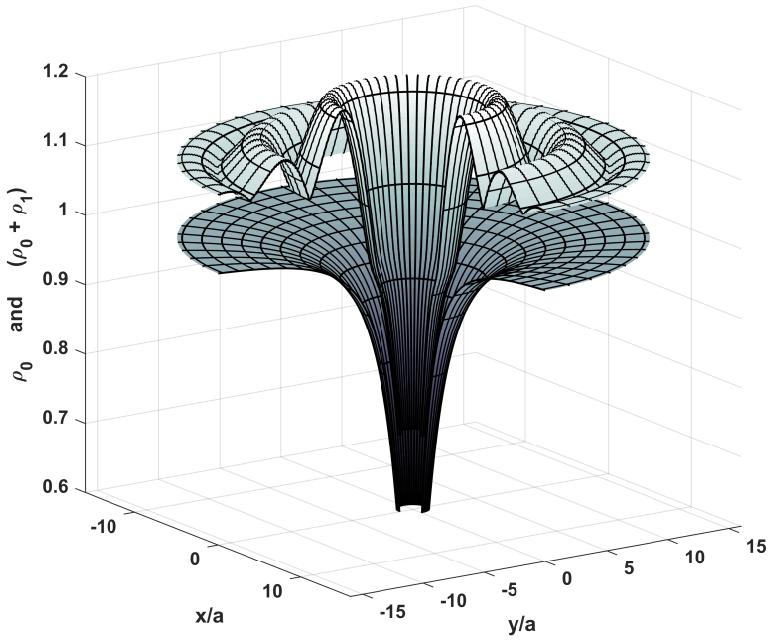

Figure 4: The self-consistent background density profile without (bottom) and with (top) superimposed density fluctuations near the vortex. The fluctuations are plotted at $t * c/a = 50$ while interacting with the event horizon. The top plot is displaced by 0.1 upward to enhance visibility.

Figure 5 is the main result of the paper. On the left, the variation of the relative energy (gain) for the superradiant and subradiant cases under const-bg-dens approximation are compared. In the subradiant case, the energy of the wave is completely absorbed by the vortex. The right panel shows the energy gain for the const-bg-dens and self-bg-dens formulations. The prominent difference is that the const-bg-dens results in an overshoot in the gain which *then* decreases as the wave is outgoing, whereas the non-constant density model reaches monotonically to a final gain value of the outgoing wave. In the self-bg-dens case, the fluctuations arrive slightly later, since the sound speed decreases near the vortex. Both formulations predict a gain of about 40%.

Finally, we investigate the spectral behavior of the superradiance. The energy gain factors achieved for acoustic fluctuations with different frequencies are plotted in Fig. 6, as obtained in const-bg-dens and self-bg-dens cases, respectively. The fluctuation wave frequency is scaled by the vortex rotation frequency, which is determined from $\vec{v_\theta} = \vec{\Omega} \times \vec{r}$ as

$$\Omega = \frac{B}{r_\hbar^2} = q\frac{\hbar}{m}\frac{1}{r_\hbar^2} = q\sqrt{2}\frac{c_\infty}{\xi} \tag{30}$$

The const-bg-dens and self-bg-dens profiles differ in the calculated superradiance mostly in the intermediate range of the scaled frequency, where the non-constant density model yielding a

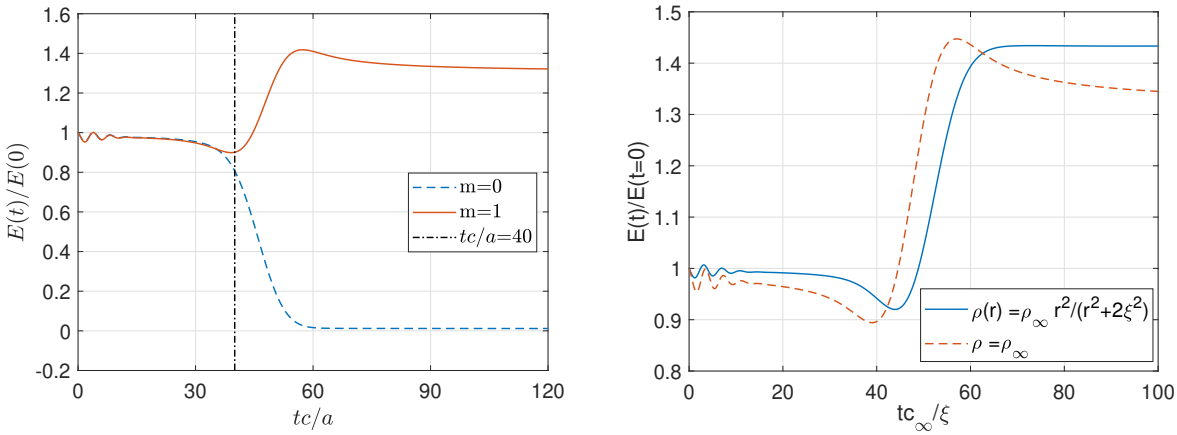

(a) (b)

Figure 5: [left] The energy gain for the superradiant ($m = 1$) (red) and the subradiant ($m = 0$) (blue) settings of the vortex. The vertical dashed line is the time the wave reaches the event horizon. [right] The energy gain under constant background density (red) and self-consistent background density (blue) formulations.

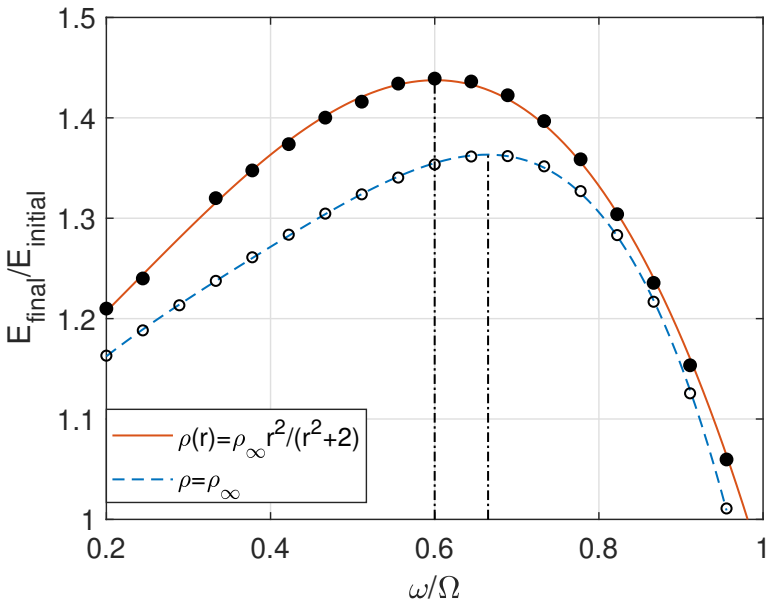

Figure 6: Superradiance as a function of the frequency of the incident acoustic perturbative wave, normalized by the vortex rotation frequency, and calculated with the constant density (circles) and self-consistent density (dots) background density profiles. Maximum gain for each case is marked by a vertical line.

slightly higher ($\sim 10\%$) gain. This is consistent with the result for single frequency shown in Fig. **??**. For low frequency perturbations, $\omega/\Omega 1$ the difference decreases but remains finite. Both models exhibit a superradiance profile biased towards the upper midrange with respective maxima attained at $\tilde{\omega} = 0.60$ and $\tilde{\omega} = 0.67$.

6. Conclusion

We performed the formulation of the acoustic superradiance with the self-consistent background density model of the BEC vortex state. The resulting dynamics of superradiance is compared with that of the constant background density approximation. The main conclusion is that the self-consistent background density eliminates the overshoot behavior of the constant density approximation in the superradiance, and provides an overall enhanced gain for the superradiance effect for the single-quantized vortex state. Moreover, the self-consistent background density formulation implies that multiquantized vortices each would have a different background density profile and thus appear as a different black-hole, as the characteristic parameters (i.e. event horizon, ergosphere) changes. The vortex rotation frequency, which can be set independently as integer multiples of a fixed value in the constant density approximation, becomes an implicit function of the background density profile and changes nontrivially for multiquantized vortices. Admittedly, these implications may become relevant after the stability issues of multiquantized vortex states are resolved experimentally. We conclude by indicating two directions in which the present formulation may be advanced. The first one is to implement dispersion effects as it is inherent to any wave propagation phenomenon. The second is to include confinement potentials as the stability of multiquantized vortices may only become available in their presence.

Acknowledgments

The authors would like to express their sincere thanks to Professor Tekin Dereli for his "superradiant" guidance throughout this study and beyond.

References

[1] Barcelo C, Liberati S and Visser M 2001 *Classical and Quantum Gravity* **18** 1137
[2] Garay L J, Anglin J, Cirac J I and Zoller P 2002 *International Journal of Theoretical Physics* **41** 2073–2090
[3] Garay L J 2001 *Physical Review A* **63** 023611
[4] Lahav O, Itah A, Blumkin A, Gordon C, Rinott S, Zayats A and Steinhauer J 2010 *Phys. Rev. Lett.* **105**(24) 240401 URL https://link.aps.org/doi/10.1103/PhysRevLett.105.240401
[5] Unruh W G 1981 *Phys. Rev. Lett.* **46**(21) 1351–1353 URL https://link.aps.org/doi/10.1103/PhysRevLett.46.1351
[6] Carlson N N 1996 *Physica D: Nonlinear Phenomena* **98** 183 – 200 ISSN 0167-2789 URL http://www.sciencedirect.com/science/article/pii/0167278996000528
[7] Fetter A L and Svidzinsky A A 2001 *Journal of Physics: Condensed Matter* **13** R135
[8] Macher J and Parentani R 2009 *Physical Review A* **80** 043601
[9] Basak S and Majumdar P 2003 *Classical and Quantum Gravity* **20** 3907
[10] Torres T, Patrick S, Coutant A, Richartz M, Tedford E W and Weinfurtner S 2017 *Nature Physics*
[11] Ghazanfari N and Müstecaplıoğlu Ö E 2014 *Physical Review A* **89** 043619
[12] Steinhauer J 2014 *Nature Physics* **10** 864
[13] Steinhauer J 2016 *Nature Physics* **12** 959
[14] Kolobov V I, Golubkov K, de Nova J R M and Steinhauer J 2021 *Nature Physics* **17** 362–367
[15] Cherubini C, Federici F, Succi S and Tosi M 2005 *Physical Review D* **72** 084016
[16] Federici F, Cherubini C, Succi S and Tosi M 2006 *Physical Review A* **73** 033604
[17] Demirkaya B, Dereli T and Güven K 2018 *arXiv preprint arXiv:1806.02139*
[18] Visser M 1998 *Classical and Quantum Gravity* **15** 1767
[19] Dalfovo F, Giorgini S, Pitaevskii L P and Stringari S 1999 *Reviews of Modern Physics* **71** 463
[20] S P 2021 *Classical Quantum Gravity* **38** 095010
[21] Desyatnikov A S, Torner L and Kivshar Y S 2005 *arXiv preprint nlin/0501026*
[22] Zhang Y, Bao W and Du Q 2007 *European Journal of Applied Mathematics* **18** 607–630
[23] Leanhardt A E *et al.* 2003 *Phys. Rev. Lett.* **90** 140403
[24] Shin Y *et al.* 2004 *Phys. Rev. Lett.* **93** 160406
[25] Huhtamaki J A M, Möttönen M and Virtanen S M M 2006 *Phys. Rev. A.* **74** 063619
[26] Leanhardt A E *et al.* 2003 *Phys. Rev. Lett.* **89** 190403
[27] Pethick C J and Smith H 2002 *Bose-Einstein Condensation in Dilute Gases* (Cambridge University Press)
[28] Berloff N G 2004 *J. Phys. A: Math Gen.* **37** 1617–1632
[29] Slatyer T R and Savage C M 2005 *Classical and Quantum Gravity* **22** 3833 URL http://stacks.iop.org/0264-9381/22/i=19/a=002

[30] Chen W *et al.* 2021 *Commun. Theor. Phys.* **73** 085701
[31] Basak S and Majumdar P 2003 *Classical and Quantum Gravity* **20** 2929
[32] Scheel M A, Erickcek A L, Burko L M, Kidder L E, Pfeiffer H P and Teukolsky S A 2004 *Physical Review D* **69** 104006
[33] Verhelst N and Tempere J *Vortex Dynamics and Optical Vortices*
[34] Anderson M H, Ensher J R, Matthews M R, Wieman C E and Cornell E A 1995 *science* **269** 198–201
[35] Alcubierre M and Brügmann B 2001 *Phys. Rev. D* **63**(10) 104006 URL `https://link.aps.org/doi/10.1103/PhysRevD.63.104006`